Lyu *et al.*
EURASIP Journal on Advances in Signal Processing (2022) 2022:113
https://doi.org/10.1186/s13634-022-00947-3

EURASIP Journal on Advances in Signal Processing

RESEARCH Open Access

Signal processing in passive radar with multi-user MIMO-OFDM signal

Xiaoyong Lyu*, Baojin Liu and Wenbing Fan

*Correspondence: iexyl@zzu.edu.cn

School of Information Engineering, Zhengzhou University, No. 100 Science Avenue, Zhengzhou 450001, China

Abstract

In this paper, we propose a signal processing method in passive radar using the multi-user (MU) multiple-input multiple-output (MIMO) orthogonal frequency division multiplexing (OFDM) signal as the illuminator of opportunity. The MU-MIMO-OFDM modulation is adopted in the fifth-generation (5G) communication. We consider the scenario where multiple mobile users share the same time–frequency resources but separate spatially in different beams formed a prior by the MU-MIMO transmitter antenna array, which is a quite general case in realistic 5G communication. A beam-by-beam matched filter is proposed for weak target sensing. Interference suppression is also discussed. The interference in this scenario is more complicated than that in the traditional passive radar. In the MU-MIMO communication system, the base station (BS) transmits multiple signals to different beam regions simultaneously for the communication between the BS and mobile users. For a specific beam region where the radar receiver is located, the interference consists of not only the direct and multipath interference (DMI) of the signal transmitted by the BS to this beam region, but also the inter-user interference (IUI) from the other beam regions. The DMI and IUI degrade the weak target detection capability significantly. In this paper, we propose a suppression method for jointly eliminating the DMI and IUI. Simulations verify the effectiveness of these methods.

Keywords: Passive radar, MU-MIMO-OFDM, Signal processing, Beam-by-beam matched filter, DMI and IUI cancellation

1 Introduction

Passive radars do not emit signals actively, but use the signals that already exist in the space as the illuminators of opportunity (IoO) for target sensing [1]. This technique offers a number of advantages. Passive radars impose no electromagnetic pollution on the environment, thus the deployment of passive radars is flexible. Passive radar network/multistatic passive radar can be readily developed, which provides great spatial diversity for improved target sensing performance [2, 3]. Moreover, passive radars are of smaller size and low cost compared with their active counterparts. Signals that can be used as IoOs in passive radar include the frequency modulation (FM) signal [4–6], analog television signal [7, 8], digital audio broadcasting (DAB)/ digital video broadcasting (DVB) signals [9–11], global system for mobile communications (GSM) signal [12,

13], satellite navigation/communication signals [14–18], wireless local area network signal (WLAN) [19–23], long-term evolution (LTE) signal [24–26], and the fifth-generation (5G) communication signal [27–29]. Among all the signals, the 5G signal has great potential for radar use, since it has large bandwidth, offering good range resolution. Furthermore, the 5G signal uses the multi-input multi-output (MIMO) orthogonal frequency division multiplexing (OFDM) technique, which provides a great degree of freedom for improved target sensing capability when used as IoO in passive radar [30, 31]. In this paper, we consider the passive radar sensing problem with the 5G signal.

Generally, a passive radar has two physical channels, i.e., reference and surveillance channels. The reference channel records the direct-path signal from the transmitter, which is used as the reference signal. The surveillance channel receives the target-reflected signals from the surveillance region of interest. It is noted that the direct and multipath interference (DMI) signals can also leak into the surveillance channel, usually from the sidelobe of the surveillance antenna. The DMI can be far stronger than the target-reflected signals [32]. The traditional passive radar signal processing method first performs clutter cancellation for suppressing the strong DMI and then conducts the range Doppler cross-correlation between the reference and surveillance signals to further increase the target signal-to-interference plus noise ratio (SINR) [33]. Potential targets are detected in the range Doppler cross-correlation surface. This method is waveform-independent and has received many successful applications in passive radars, including the 5G signal-based passive radar [28, 29]. However, the waveform-independent processing method operates with the originally digitized signals, which usually have luge data size, especially for signals with large bandwidths such as the 5G signal. Clutter cancellation and range Doppler cross-correlation with the originally digitized signals take huge computational time and require large storage capability. Moreover, methods in [28, 29] do not consider the inter-users interference (IUI) which is induced because of the multi-user MIMO-OFDM (MU-MIMO-OFDM) technique exploited by the 5G communication. Recently, the channel estimate-based signal processing method proposed in the OFDM-based passive radar has attracted much attention [34–36]. This method first obtains the channel estimate with the originally digitized signals and then performs target sensing based on the channel estimate. The data size of the channel estimate is significantly reduced compared with that of the originally digitized signal, and processing with the channel estimate can be implemented with fast Fourier transform (FFT). This increases the computational efficiency significantly. However, the traditional OFDM passive radar assumes that only one data symbol is modulated in one subcarrier per OFDM block, which is not the case for a 5G signal. The 5G communication exploits the MU-MIMO-OFDM technique, where the base station (BS) antenna array forms several radial beams, and each beam covers a radial sector providing the communication link to the users in that sector [37]. Users in different beams can share the same time and frequency resources, but only separate spatially. In this circumstance, multiple data symbols may correspond to the same time–frequency grid. The traditional channel estimate-based processing method in OFDM passive radar cannot be used here straightforwardly. Additionally, there exists IUI in MU-MIMO-OFDM system; thus, the interference in MU-MIMO-OFDM passive radar includes not only the DMI, but also

the IUI. The IUI may not be a problem for communication, because it is usually weaker compared to the desired signal transmitted to the mobile users. Moreover, techniques such as the orthogonal signal design, precoder, and linear minimum mean square error (LMMSE) equalization, can also be used to mitigate the IUI [38]. However, the IUI may impose a significant influence on passive radar sensing, since the IUI may be far stronger than the target-reflected signals. The treatment of IUI has not been discussed previously.

Sensing with the MU-MIMO-OFDM signal has also been discussed in the joint communication and radar sensing community, where the compressed sensing and signal stripping methods (SSM) have been proposed for target parameter estimation [39, 40]. The compressed sensing method in [39] first exploits one OFDM block for target delay estimation. The other parameters are estimated subsequentially when the delays are obtained. This method works for targets with large signal-to-noise ratios (SNRs). However, for small targets, the integration length of only one OFDM block may not be sufficient for the targets to be detected. The compressed sensing framework can also be extended with multiple OFDM blocks for delay estimation; however, in this case the method will have huge computational complexity. The SSM first removes the data symbols from the channel estimate model and then performs target parameter estimation. However, the data symbol stripping operation usually amplifies the noise, as can be seen from the analysis in this paper. Both [39] and [40] use the background subtraction method for interference cancellation. However, this method proposed therein relies on accurate data symbol removal from the signal model, which is not easy to achieve in MU-MIMO-OFDM where multiple users share the same time–frequency resources but only separate spatially.

In this paper, we consider the passive radar sensing problem with the MU-MIMO-OFDM signal. We develop the signal processing method based on the channel estimate model, which is established under the assumption that the beamforming is enabled by the BS. Based on this model, we propose a beam-by-beam matched filter (BBB-MF) method for target sensing. Compared with the compressed sensing method in [39], the proposed method uses multiple OFDM blocks for target sensing, which obviously has greater sensing capability for weak targets. Moreover, the proposed method can be implemented by FFT and thus has higher computational efficiency. Compared with the SSM in [40], the proposed method does not remove the data symbols from the signal model but compensates the channel estimate model with the conjugate data symbols. The proposed method has a lower interference floor in the matched filter map. Compared with the traditional OFDM passive radar method in [34–36], the proposed BBB-MF considers the scenario where multi-users share the same time–frequency resources. In this paper, we also analyze the influence of the IUI on target detection and propose a cancellation method for the joint reduction of the DMI and IUI. The joint reduction method does not rely on the removal of data symbols from the signal model.

The organization of the rest of the paper is as follows: Sect. 2 derives the signal model. Section 3 introduces the BBB-MF and discusses the DMI and IUI cancellation. Section 4 provides the simulations and corresponding discussions. Section 5 gives the conclusion.

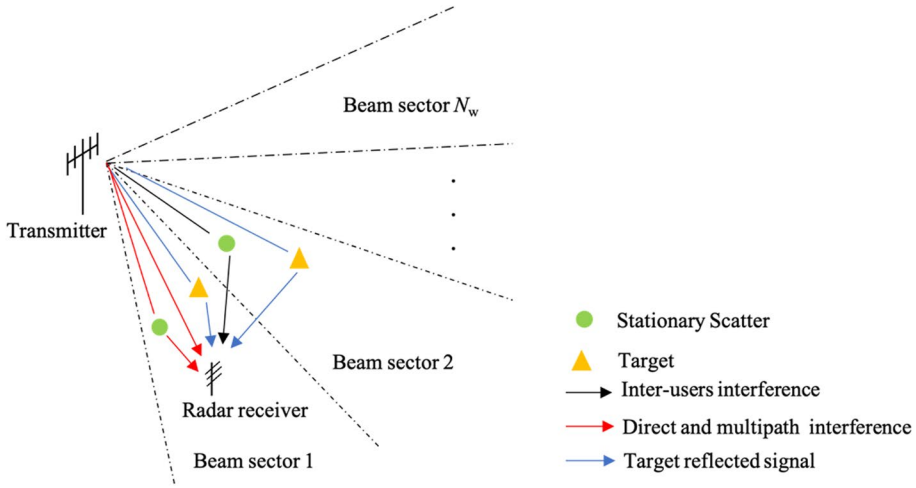

Fig. 1 MU-MIMO-OFDM passive radar

2 Signal model

Consider a MU-MIMO-OFDM passive radar system shown in Fig. 1.

The BS is assumed to be equipped with an M-element antenna array. For MU-MIMO-OFDM communication, a fixed number of beams are formed by using the digital beamforming technique. Each beam covers a radial sector within the coverage area of the BS, providing a communication link between the BS and users in that sector. The communication cell is thus divided into several radial sectors through these beams. The beams are predefined and each has an individual weight that is stored previously in memory and it is not changed. A specific user equipment selects the best beam for communication. This beamforming scheme is named the "grid of beam (GoB)" beamforming, which is under investigation to be used with the 5G communication systems [37]. We assume that the users in different beam sectors share the same time–frequency resources, but separate spatially in different beams, which is a quite challenging scenario for passive radar sensing, because of the IUI between different beams. The IUI may not be a problem for communication, because the IUI from the other beams is weaker compared to the direct signal in the beam of interest. Moreover, techniques such as the orthogonal signal design, precoder, and linear minimum mean square error (LMMSE) equalization can also be used to mitigate the IUI. However, the IUI will impose a significant influence on passive radar sensing, since the IUI is far stronger than the target-reflected signals.

The base band signal of the MU-MIMO-OFDM system can be modeled as:

$$\mathbf{x}(t) = \sum_{b=1}^{N_w} \mathbf{w}_b r_b(t) + \mathbf{n}_x(t) \tag{1}$$

where $\mathbf{w}_b$ is the weight vector of the bth beam and N_w is the number of beams.$r_b(t)$ is the OFDM signal transmitted to the bth beam sector and can be written as:

$$r_b(t) = \sum_{k} \sum_{n=-N/2}^{N/2-1} s_b^k(n) e^{j2\pi n \Delta f (t-kT_o)} q(t-kT_o) \tag{2}$$

where $s_b^k(n)$ is the data symbol at the nth subcarrier of the kth OFDM block. Δf is the subcarrier spacing. N is the number of subcarriers at each OFDM block. Then, the bandwidth of the signal is $N\Delta f$. q(t) is expressed as:

$$q(t) = \begin{array}{l} 1 \ t \in [-T_{cp}, T] \\ 0 \ \text{otherwise} \end{array} \tag{3}$$

T is the length of the OFDM useful signal in one OFDM block and $T{=}1/\Delta f$ to make sure that the subcarrier frequencies are orthogonal.T_{cp} is the length of the cyclic prefix. $T_o = T_{cp} + T$ is the length of one OFDM block. $\mathbf{n}_x(t)$ is the additive noise.

The signal received by the radar receiver with a single antenna element can be represented as:

$$\begin{aligned} y(t) &= \sum_{i=1}^{N_c} A_i \mathbf{a}^T(\theta_i)\mathbf{x}(t-\tau_i) + \sum_{i=1}^{N_t} A_i^e \mathbf{a}^T(\theta_i^e)\mathbf{x}(t-\tau_i^e)e^{j2\pi f_{d,i}t} + n_y(t) \\ &= \sum_{b=1}^{N_w}\sum_{i=1}^{N_c} A_i \mathbf{a}^T(\theta_i)\mathbf{w}_b r_b(t-\tau_i) + \sum_{b=1}^{N_w}\sum_{i=1}^{N_t} A_i^e \mathbf{a}^T(\theta_i^e)\mathbf{w}_b r_b(t-\tau_i^e)e^{j2\pi f_{d,i}t} + n_y(t) \end{aligned} \tag{4}$$

where A_i and τ_i are the amplitude and delay of the ith clutter signal, respectively. θ_i is the angle of departure (AOD) of the ith clutter signal. N_c is the number of clutter signals. $\mathbf{a}(\cdot)$ is the steering vector of the transmit antenna array. $(\cdot)^T$ means taking the transpose of the matrix. A_i^e, τ_i^e, and $f_{d,i}$ are the amplitude, delay, and Doppler frequency of the ith target-reflected signal, respectively. θ_i^e is the AOD of the ith target-reflected signal. N_t is the number of target-reflected signals. $n_y(t)$ is the additive noise. It is noted that the signal model in (4) and the corresponding signal processing methods developed later can be extended to the multiple receive antenna elements case straightforwardly.

Assume that the radar receiver is accurately synchronized with the MU-MIMO-OFDM transmitter, and the largest possible delay of the clutter and target-reflected signals is smaller than the cyclic prefix $\tau_{\max} < T_{cp}$. The channel estimate of the nth subcarrier in the kth OFDM block can be obtained as:

$$H_n^k = \frac{1}{T}\int_0^T e^{-j2\pi n\Delta f t} y(t + kT_o)dt \tag{5}$$

In order to calculate (5), we first examine the phase rotation term corresponding to the Doppler shift in (4). Since the product between T_o and the Doppler frequency f_d is usually far smaller than unity, the phase rotation within one OFDM block can be approximated as:

$$e^{j2\pi f_{d,t} t} \approx e^{j2\pi f_{d,t}(T/2)}, t \in [0, T] \tag{6}$$

Furthermore, all subcarrier frequencies are orthogonal, i.e.,

$$\int_0^T e^{-j2\pi n\Delta f t} e^{j2\pi m\Delta f t} dt = 0, m \neq n \tag{7}$$

Substituting (4) into (5), and combining (6) and (7), we can express the channel estimate as:

$$
\begin{aligned}
H_n^k \approx & \sum_{b=1}^{N_w}\sum_{i=1}^{N_c} A_i \mathbf{a}^T(\theta_i)\mathbf{w}_b s_b^k(n) e^{-j2\pi n\Delta f \tau_i} \\
& + \sum_{b=1}^{N_w}\sum_{i=1}^{N_t} A_i^e \mathbf{a}^T(\theta_i^e)\mathbf{w}_b s_b^k(n) e^{-j2\pi n\Delta f \tau_i^e} e^{j2\pi f_{d,i} k T_o} + n_n^k
\end{aligned}
\tag{8}
$$

where n_n^k is the channel estimate noise. It is noted that the phase constant for each target is included into the amplitude. In the following, we will examine each term in (8). Without loss of generality, we assume that the radar receiver locates within the first beam sector. Then, (8) can be rewritten as:

$$
\begin{aligned}
H_n^k \approx & \sum_{i=1}^{N_c} A_i \mathbf{a}^T(\theta_i)\mathbf{w}_1 s_1^k(n) e^{-j2\pi n\Delta f \tau_i} \\
& + \sum_{i=1}^{N_t} A_i^e \mathbf{a}^T(\theta_i^e)\mathbf{w}_1 s_1^k(n) e^{-j2\pi n\Delta f \tau_i^e} e^{j2\pi f_{d,i} k T_o} \\
& + \sum_{b=2}^{N_w}\sum_{i=1}^{N_c} A_i \mathbf{a}^T(\theta_i)\mathbf{w}_b s_b^k(n) e^{-j2\pi n\Delta f \tau_i} \\
& + \sum_{b=2}^{N_w}\sum_{i=1}^{N_t} A_i^e \mathbf{a}^T(\theta_i^e)\mathbf{w}_b s_b^k(n) e^{-j2\pi n\Delta f \tau_i^e} e^{j2\pi f_{d,i} k T_o} + n_n^k
\end{aligned}
\tag{9}
$$

where the first term in (9) is the DMI, i.e., the clutter-reflected signals corresponding to the transmitted signal to the first beam sector. The second term is the target-reflected signals. The third term is the IUI, i.e., the clutter-reflected signals corresponding to the transmitted signal to the other beam sectors (not including the first beam sector). The last term is the target-reflected signals corresponding to the transmitted signals to the other beam sectors (not including the first beam sector). Usually, the DMI and IUI are far stronger than the target-reflected signals and thus have a significant influence on target detection. In the following, we will develop the BBB-MF and interference cancellation methods based on model (9).

3 Methods

3.1 Beam-by-beam matched filter (BBB-MF)

We first discard the DMI and IUI, then (9) can be rewritten as:

$$
\begin{aligned}
H_n^k \approx & \sum_{i=1}^{N_t} A_i^e \mathbf{a}^T(\theta_i^e)\mathbf{w}_1 s_1^k(n) e^{-j2\pi n\Delta f \tau_i^e} e^{j2\pi f_{d,i} k T_o} \\
& + \sum_{b=2}^{N_w}\sum_{i=1}^{N_t} A_i^e \mathbf{a}^T(\theta_i^e)\mathbf{w}_b s_b^k(n) e^{-j2\pi n\Delta f \tau_i^e} e^{j2\pi f_{d,i} k T_o} + n_n^k
\end{aligned}
\tag{10}
$$

Since $\mathbf{w}_1 s_1^k(n)$ is the signal transmitted to the first beam sector, where the radar receiver is located, the direct-path signal associated with $\mathbf{w}_1 s_1^k(n)$ usually has large SINR. Therefore, we assume that $s_1^k(n)$ can be decoded by the radar receiver. With $s_1^k(n)$, the matched filter of the first beam sector is developed as:

$$\chi_1(\tau,f_d)=\sum_{k=1}^{K}\sum_{n=-N/2}^{N/2-1}H_n^k\left(s_1^k(n)\right)^* e^{j2\pi n\Delta f\tau}e^{-j2\pi f_d kT_o} \tag{11}$$

where $(\cdot)^*$ means taking the complex conjugate of the entity. K is the number of OFDM blocks within the coherent processing interval (CPI). It is ready to see that (11) can be implemented with the 2D Fourier transform of H_n^k compensated by $\left(s_1^k(n)\right)^*$. By properly choosing the numbers of subcarriers and OFDM blocks for processing, fast Fourier transform (FFT) can be used to increase the computational efficiency.

It is noted that the SSM proposed in [40] first removes data symbols from the channel estimate and then performs the 2D FFT. The SSM is expressed as:

$$\chi_1^{\text{strip}}(\tau,f_d)=\sum_{k=1}^{K}\sum_{n=-N/2}^{N/2}\frac{H_n^k}{s_1^k(n)}e^{j2\pi n\Delta f\tau}e^{-j2\pi f_d kT_o} \tag{12}$$

It is seen from (10) and (12) that the data symbols cannot be removed completely in the MU-MIMO-OFDM passive radar. Moreover, the SSM can amplify the noise, as can be seen in the later simulations.

In the following, we take a deep insight into (11), which is rewritten as:

$$\begin{aligned}&\chi_1(\tau,f_d)\\&=\sum_{i=1}^{N_t}A_i^e\mathbf{a}^T(\theta_i^e)\mathbf{w}_1\sum_{k=1}^{K}\sum_{n=-N/2}^{N/2-1}\left|s_1^k(n)\right|^2 e^{-j2\pi n\Delta f(\tau_i^e-\tau)}e^{j2\pi(f_{d,i}-f_d)kT_o}\\&+\sum_{b=2}^{N_w}\sum_{i=1}^{N_t}A_i^e\mathbf{a}^T(\theta_i^e)\mathbf{w}_b\sum_{k=1}^{K}\sum_{n=-N/2}^{N/2-1}\left(s_1^k(n)\right)^* s_b^k(n)e^{-j2\pi n\Delta f(\tau_i^e-\tau)}e^{j2\pi(f_{d,i}-f_d)kT_o}+n_g\end{aligned} \tag{13}$$

It is reasonable to assume that the data symbols transmitted are random. That is, $s_b^k(n)$ is statistically independent for different subcarrier n, OFDM block k, and beam sector b. For a specific modulation, such as the quadrature phase shift keying (QPSK), 64-quadrature amplitude modulation (64-QAM), and 256-QAM, we have

$$\sum_{k=1}^{K}\sum_{n=-N/2}^{N/2-1}\left(s_1^k(n)\right)^* s_b^k(n)\ll\sum_{k=1}^{K}\sum_{n=-N/2}^{N/2-1}\left|s_1^k(n)\right|^2 \tag{14}$$

Then, the second term in (13) is significantly smaller than the first term and can be discarded. That is, the influence of the target-reflected signals corresponding to the transmitted signals to the other beam sectors can be ignored. For a specific target located in the delay and Doppler cell $(\tau_l^e,f_{d,l})$, the matched filter result at this cell can be represented as:

$$\chi_1(\tau_l^e,f_{d,l})=A_l^e\mathbf{a}^T(\theta_l^e)\mathbf{w}_1\sum_{k=1}^{K}\sum_{n=-N/2}^{N/2-1}\left|s_1^k(n)\right|^2+n_1(\tau_l^e,f_{d,l}) \tag{15}$$

where $\sum_{k=1}^{K}\sum_{n=-N/2}^{N/2-1}\left|s_1^k(n)\right|^2$ corresponds to the integration gain, the magnitude of which is proportional to the product of the signal bandwidth and length. For 5G signal with

typical bandwidth of 50–100 MHz, this integration gain can be very high. $\mathbf{a}^T(\theta_l^e)\mathbf{w}_1$ corresponds to the gain of beamforming. Specifically, for an M-element antenna array, the SNR increase because of the beamforming can be expressed as $20\log\left(\left|\mathbf{a}^T(\theta_l^e)\mathbf{w}_1\right|/\sqrt{M}\right)$. When the target locates within the first beam sector, $20\log\left(\left|\mathbf{a}^T(\theta_l^e)\mathbf{w}_1\right|/\sqrt{M}\right)$ has a large gain. In this case, the target energy can increase further. $n_1(\tau_l^e, f_{d,j})$ includes the noise term, the DMI and IUI residual, the sidelobes from the other targets and the target interference from the other beams (i.e., the second term in (13)). When the target after processing has sufficient SINR, it will be detected on the 2-d map of the matched filter. However, it is noted that the beamforming gain $20\log\left(\left|\mathbf{a}^T(\theta_l^e)\mathbf{w}_1\right|/\sqrt{M}\right)$ will be smaller for targets locating in the other beam sectors than the first beam sector. What was worse, $20\log\left(\left|\mathbf{a}^T(\theta_l^e)\mathbf{w}_1\right|/\sqrt{M}\right)$ may be even smaller than zero. In this case, the SINR will decrease. It is concluded that the matched filter of the first beam sector can have better target detection performance for the targets within the first beam sector, but degrades for the targets locating in the other beam sectors.

For the targets locating in the other beam sectors than the first beam sector, the data symbols transmitted in their beam sectors can be used to develop the matched filters. This results in the BBB-MF. That is, we use $s_b^k(n)$ to develop the matched filter for the bth beam sector, for $b = 1, 2, ..., N_w$, and each matched filter is designed similarly with (11). As the matched filter of the first beam sector, each matched filter can have good detection performance for targets in its corresponding beam sector. Performing the matched filtering beam by beam is similar to beam scanning in traditional radars. The diagram of the BBB-MF is shown in Fig. 2.

It is noted that obtaining the data symbols in the other beam sectors than the first beam sectors is not easy, but not impossible. In cooperative passive radars [41] or joint communication and radar systems, all the data symbols transmitted by the BS can be known. In a passive radar network, multiple radar receivers can be exploited and each beam sector can be deployed with one radar receiver. The radar receivers can communicate the data symbols they obtain. In GoB-based beamforming, the beam sectors are defined globally and not changed. Therefore, the deployment of radar receivers in each beam sector is possible.

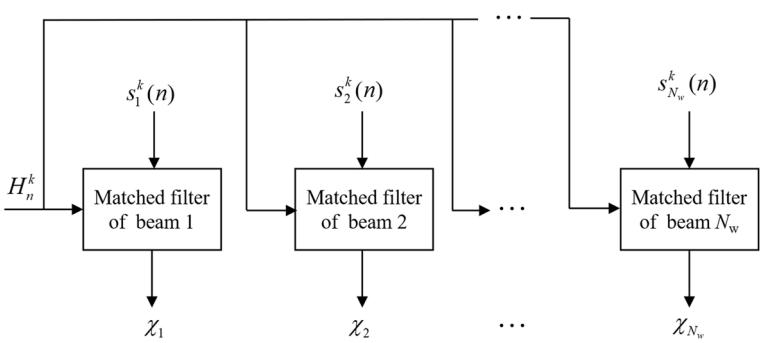

Fig. 2 Diagram of the BBB-MF

3.2 DMI and IUI cancellation

In this section, we discuss the cancellation of DMI and IUI. It is known in passive radar that the DMI has a big influence on target detection, because the DMI is far stronger than the target-reflected signals. In MU-MIMO-OFDM passive radar, apart from the DMI, the IUI also imposes a significant impact on target detection, since the IUI, i.e., the clutter-reflected signals corresponding to the transmitted signal to the other beam sectors, can also be significantly larger than the target echoes. In the following, we propose a joint cancellation method for suppressing the DMI and IUI.

Since the target-reflected signals are far weaker than the DMI and IUI, the target-reflected signal terms in (9) can be discarded when dealing with the DMI and IUI cancellation. Furthermore, the beamforming gain $\mathbf{a}^T(\theta_i)\mathbf{w}_b$ can be included in the amplitude. Then, (9) can be rewritten as:

$$H_n^k \approx \sum_{b=1}^{N_w}\sum_{i=1}^{N_c} B_b^i s_b^k(n) e^{-j2\pi n\Delta f \tau_i} + n_n^k \tag{16}$$

where $B_b^i = A_i \mathbf{a}^T(\theta_i)\mathbf{w}_b, b = 1, 2, ..., N_w$. Encapsulate H_n^k into a vector as:

$$\mathbf{H} = \left[H_{-N/2}^1, H_{-N/2}^2, ..., H_{-N/2}^K, H_{-N/2+1}^1, H_{-N/2+1}^2, ..., H_{N/2-1}^K\right]^T \tag{17}$$

Quantify the delay τ into a number of grids, with $\Delta\tau$ denoting the delay spacing between two adjacent grids, and formulate the measurement matrix in the following:

$$\mathbf{U} = \left[\mathbf{U}_1, \mathbf{U}_2, ..., \mathbf{U}_{N_w}\right]^T \tag{18}$$

where

$$\mathbf{U}_b = [\mathbf{u}_b^1, \mathbf{u}_b^2, ...\mathbf{u}_b^P] \tag{19}$$

$$\mathbf{u}_b^p = \begin{bmatrix} \mathbf{s}_b(-N/2)e^{-j2\pi\Delta f(-N/2)\tau_p} \\ \mathbf{s}_b(-N/2+1)e^{-j2\pi\Delta f(-N/2+1)\tau_p} \\ \vdots \\ \mathbf{s}_b(N/2-1)e^{-j2\pi\Delta f(N/2-1)\tau_p} \end{bmatrix} \tag{20}$$

$$\mathbf{s}_b(n) = \left[s_b^1(n), s_b^2(n), ..., s_b^K(n)\right]^T \tag{21}$$

$\tau_p = p\Delta\tau, p = 1, 2, ..., P$, with $P\Delta\tau$ denoting the maximum delay of the DMI or IUI to be cancelled. Combining (16) to (21), we have:

$$\mathbf{H} = \mathbf{UB} + \mathbf{n} \tag{22}$$

where $\mathbf{B} = [B_1, B_2, ...]^T$ represents the amplitude of the potential DMI and IUI. $\mathbf{n}$ is the noise. Then, the amplitude of the DMI and IUI can be estimated using the least square technique, i.e.,

$$\hat{\mathbf{B}} = \arg\min_{\mathbf{B}} \|\mathbf{H} - \mathbf{UB}\|_2^2 \tag{23}$$

where $\|\cdot\|_2$ is the l_2 norm of the entity. The amplitude vector $\mathbf{B}$ is estimated by solving (23) as:

$$\hat{\mathbf{B}} \approx \left(\mathbf{U}^H\mathbf{U}\right)^{-1}\mathbf{U}^H\mathbf{H} \tag{24}$$

where $(\cdot)^H$ means taking the conjugate transpose of the entity. It is noted that, when the delay grid spacing $\Delta\tau$ is small, the matrix $\mathbf{U}^H\mathbf{U}$ may be singular, then the matrix inversion in (24) will lead to numerical problem. The diagonal loading technique can be exploited to overcome this problem. Then, (24) can be further represented as:

$$\hat{\mathbf{B}} \approx \left(\mathbf{U}^H\mathbf{U}+\lambda\mathbf{I}\right)^{-1}\mathbf{U}^H\mathbf{H} \tag{25}$$

where λ is a small positive constant. The value of λ can be selected by inspecting the eigenvalues of the matrix $\mathbf{U}^H\mathbf{U}$. Traditionally, it is chosen higher than the nonsignificant eigenvalues, but lower than the smallest significant eigenvalue of the matrix $\mathbf{U}^H\mathbf{U}$. Diagonal loading is equivalent to imposing a constraint on the l_2 norm of the amplitude vector $\mathbf{B}$ when using (23) to estimate $\mathbf{B}$, i.e.,

$$\hat{\mathbf{B}}= \arg\min_{\mathbf{B}} \left\{ \|\mathbf{H}-\mathbf{U}\mathbf{B}\|_2^2 + \lambda\|\mathbf{B}\|_2^2 \right\} \tag{26}$$

Solving (26) can get the same result with (25). The DMI and IUI can be cancelled as:

$$\mathbf{H}_{\text{remain}} = \mathbf{H} - \mathbf{U}\hat{\mathbf{B}} \tag{27}$$

where $\mathbf{H}_{\text{remain}}$ is the remaining signal after DMI and IUI cancellation.

The proposed DMI and IUI cancellation method is similar to the extensive cancellation method (ECA) in passive radar [40], except that the proposed method operates with the channel estimate H_n^k, but the ECA performs in the original digital data domain. The MU-MIMO-OFDM signal usually has great bandwidth, thus the sampling frequency is large, leading to huge data size in the original digital data domain. Cancellation in the original digital data domain has huge computational complexity and requires large storage capability. However, the data size of the channel estimate H_n^k is significantly smaller; therefore, operating with H_n^k increases the computational efficiency greatly. Similar to the parallel implementation version of ECA, i.e., the batch-ECA [42], where the received signal is divided into several segments and the cancellation is performed segment by segment, the proposed method can also be performed segment by segment by properly arranging the channel estimate H_n^k. This can further increase the computational efficiency.

4 Results and discussion

In this section, we test the proposed methods through simulations. The signal parameters are set according to the 5G signal protocol "3GPP release 15" and summarized in Table 1 [30]. It can be seen from Table 1 that the carrier frequency is set to 3.5 GHz. The bandwidth is set to 50 MHz. The subcarrier frequency spacing is 15 kHz. The total number of subcarriers per OFDM block is 3333. Fourteen OFDM blocks form a subframe with a length of 1 ms. Thus, the length of each OFDM block is 71.4us. In each OFDM

Table 1 Signal parameters

Item	Value
Carrier frequency	3.5 GHz
Bandwidth	50 MHz
Subcarrier frequency spacing	15 kHz
Number of subcarriers per OFDM block	3333
Length of each OFDM block	71.4 us
Length of CP	4.7 us
CPI	0.1 s

Table 2 Stationary scatter parameters

	Bistatic range, m	AOD, °	SNR, dB
Direct signal	100	33	20
Scatter 1	210.6	88	15
Scatter 2	300.3	65	7

block, the length of useful OFDM signal is 66.7 us and the length of CP is 4.7us, which corresponds to a maximum bistatic range of 1.4 km. The CPI is set to 0.1 s.

We assume that an eight-element uniform linear array is exploited by the transmitter, and three beam sectors are simulated with the center angles of 30°, 60°, and 90°, respectively. The beamforming weight vectors $\mathbf{w}_i$ of the three beam sectors are simulated as the conjugate steering vectors at the three center angles, i.e., $\mathbf{w}_1=\mathbf{a}^*(30°)$, $\mathbf{w}_2=\mathbf{a}^*(60°)$, $\mathbf{w}_3=\mathbf{a}^*(90°)$. 256-QAM is adopted. The data symbols in each subcarrier frequency of each OFDM block for each beam sector are generated randomly.

The passive radar receiver is located in the first beam sector and is 100 m away from the transmitter. A single-element antenna is used for signal receiving.

One direct and two stationary scatters are set, with the parameters given in Table 2.

It is noted that the SNRs in Table 2 are those before integration and beamforming. That is, for scatter i, the SNR is defined as

$$\mathrm{SNR}_i = E_{A_i\mathbf{x}_1(t-\tau_i)}/E_{n_y(t)} \tag{28}$$

where $E_{A_i\mathbf{x}_1(t-\tau_i)}$ is the energy of signal $A_i\mathbf{x}_1(t-\tau_i)$ shown in (4). $\mathbf{x}_1(t-\tau_i)$ corresponds to the transmitted signal of the first antenna array element, i.e., the first entity of signal vector $\mathbf{x}(t-\tau_i)$. Without loss of generality, the signal energy transmitted by each antenna array element is approximately the same. $E_{n_y(t)}$ is the energy of the noise in (4).

Four targets are simulated, of which the parameters are given in Table 3.

The target SNRs in Table 3 are also those before integration and beamforming. It can be seen from Table 3 that targets 1 and 2 are in the first beam sector. Target 1 is a weak target with an SNR of only − 35 dB, and target 2 is a strong target with an SNR of − 12 dB. Target 3 is in the second beam sector with an SNR of only − 30 dB. Target 4 is in the third beam sector with an SNR of − 10 dB.

The received signal by the radar receiver is simulated as (4), and Eq. (5) is performed to get the channel estimate H_n^k. Then, the DMI and IUI cancellation method in

Table 3 Target parameters

	Bistatic range, m	Doppler frequency, Hz	AOD, °	SNR, dB
Target 1	800	− 303.3	27	− 35
Target 2	400.5	210	32	− 12
Target 3	612.2	116.7	56	− 30
Target 4	300.7	163.3	92	− 10

Table 4 Predicted SNR

	Matched filter of Beam 1	Matched filter of Beam 2	Matched filter of Beam 3
Target 1	29.4	16.1	11.4
Target 2	52.5	39.7	34.2
Target 3	19.5	33.8	15.4
Target 4	36.1	31.6	54.3

subsection 3.2 is exploited for clutter signal suppression. The BBB-MF in subsection 3.1 is utilized for target detection.

It is noted that, since the channel estimate corresponding to each subcarrier in each OFDM block can be obtained separately, as shown in (5), processing with the channel estimate can be very flexible. That is, we can only pick out some of the channel estimates for processing, in order to further decrease the computational complexity. In the simulations, we decimate one OFDM block every 14 OFDM blocks. That is, we only pick out one OFDM block per subframe for processing, which corresponds to an unambiguous Doppler frequency range of [-500 Hz, 500 Hz]. In each OFDM block selected, all the subcarriers are exploited for processing to guarantee a high-range resolution, which is calculated as 3 m in this simulation. Of course, decimation can lead to a decrease in the processing gain. It can be predicted that, with decimation, the processing gain of a potential target for the matched filter of beam b can be expressed as:

$$G_b = 10\log BT_{cpi} - 10\log F_{deci} + 20\log\left(\left|\mathbf{a}^T(\theta)\mathbf{w}_b\right|/\sqrt{M}\right) \tag{29}$$

where B is the bandwidth of the signal and T_{cpi} is the length of the CPI. $10\log \mathrm{BT}_{\mathrm{cpi}}$ corresponds to the integration gain. F_{deci} is the decimation factor. $10\log F_{\mathrm{deci}}$ corresponds to the processing gain loss associated with the decimation. $20\log\left(\left|\mathbf{a}^T(\theta)\mathbf{w}_b\right|/\sqrt{M}\right)$ is the beamforming gain for beam b. M is the antenna array element number. For the setup in this simulation, the integration gain is calculated as 67 dB and the gain loss associated with the decimation is 11.5 dB (the decimation factor is 14). The maximum beamforming gain is 9 dB. It is noted that the real achieved processing gain will be smaller than that predicted in (29). This is because the $n_1(\tau_l^e, f_{d,j})$ in (15) includes not only the noise term, but also the DMI and IUI residual, the sidelobes from the other targets and the target interference from the other beams (i.e., the second term in (13)), which will increase the noise floor.

The predicted SNRs of the four targets after processing are given in Table 4.

Figure 3 shows the BBB-MF results.

It can be seen from Fig. 3 that targets 2 and 4 can be clearly seen in each matched filter map of the three beams. It can be seen from Table 4 that the predicted SNRs of the two targets after processing are sufficiently large for the three beams. That is, the predicted SNRs of target 2 are 52.5 dB, 39.7 dB, and 34.2 dB, respectively, for the three beams. The predicted SNRs of target 4 for the three beams are 36.1 dB, 31.6 dB, and 54.3 dB, respectively, for the three beams. Owing to such large predicted SNRs, the two targets can be clearly detected by each matched filter of the three beams. The real achieved SNR of a specific target after processing can be measured as:

$$SNR_{\text{mea}} = \frac{\left|\chi_b(\tau_l^e, f_{d,l})\right|}{\sqrt{\sum_{(\tau,f_d)\in \text{Cell\_Inf}} \left|\chi_b(\tau, f_d)\right|^2 / N_{\text{Cell\_Inf}}}} \tag{30}$$

where $\chi_b(\tau_l^e, f_{d,l})$ is the matched filter result at the range Doppler cell of the target. Cell_Inf is the cell area where there are no targets, which is used to calculate the interference floor of the matched filter map. $N_{\text{Cell\_Inf}}$ is the number of cells within Cell_Inf.

The real measured SNRs of target 2 and target 4 are given in Table 5. It can be seen from Tables 4 and 5 that the real measured SNRs of targets 2 and 4 are slightly smaller than the predicted ones, which is consistent with the analysis above.

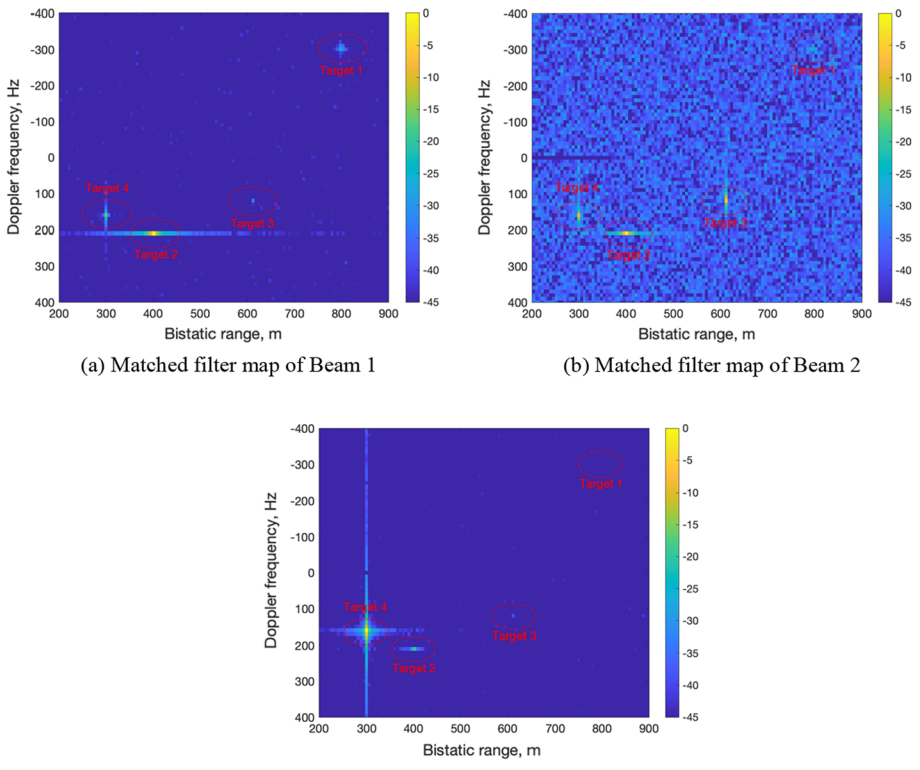

(a) Matched filter map of Beam 1

(b) Matched filter map of Beam 2

(c) Matched filter map of Beam 3

Fig. 3 BBB-MF results

Table 5 Measured SNR

	Matcher filter of Beam 1	Matcher filter of Beam 2	Matcher filter of Beam 3
Target 1	25.2	11.2	6.4
Target 2	50.2	36.2	32.2
Target 3	16.7	30	12.8
Target 4	32.8	27.7	51.6

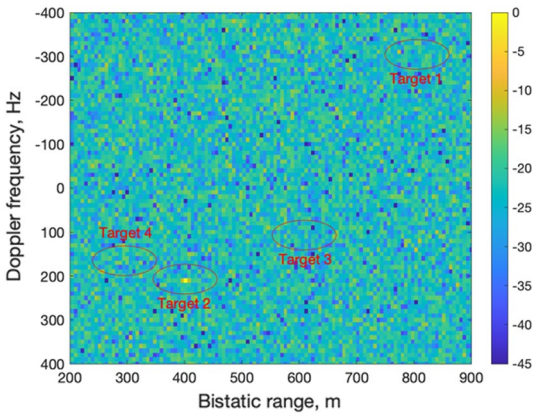

Fig. 4 Matched filter map of beam 1 with only DMI cancelled

It can be seen from Fig. 3 that target 1 can be clearly seen in the matched filter map of beam 1, but is only weakly visible within the matched filter map of beam 2. This is consistent with the predicted SNRs of the target for the two beams, i.e., 29.4 dB for beam 1 and 16.1 dB for beam 2. The measured SNRs of target 1 for the two beams are given in Table 5. It can be seen that the measured SNRs are 25.2 dB and 11.2 dB, smaller than the predicted ones. Moreover, the difference between the predicted and measured SNRs for target 1 is bigger than those for targets 2 and 4. This is reasonable, since target 1 is a small target, and the SNR of the small target can be impacted more severely by the DMI and IUI residual, the target interference from the other beams, and especially the sidelobes from the strong targets. Furthermore, for small target, $\left|\chi_b(\tau_l^e, f_{d,l})\right|$ in (30) cannot accurately represent the energy of the target. Therefore, the accuracy of (30) will decrease when using it to represent the real achieved SNR. Target 1 is not visible in the matched filter map of beam 3. This is because the predicted SNR is 11.4 dB and the measured one is only 6.4 dB for beam 3, which is not big enough compared to the fluctuation of the interference floor, leading to the invisibility of the target [33].

Target 3 is clearly seen in the matched filter map of beam 2, but is relatively weaker in the matched filter maps of beams 2 and 3. This is consistent with the predicted SNRs for the three beams, i.e., 19.5 dB, 33.8 dB, and 15.4 dB. The measured SNRs are shown in Table 5. It can be seen that the measured SNRs are smaller than the predicted ones.

Figure 4 shows the matched filter result only using the data symbols decoded from the first beam sector for processing, where the radar receiver is located. The data symbols transmitted to the other beam sectors are assumed not known. In this circumstance,

only the DMI can be suppressed, but the IUI cannot be eliminated. Meanwhile, only the matched filter of beam 1 can be performed. It can be seen that only target 2 is visible in the matched filter map. The other targets are not visible in the figure. Moreover, the interference floor shown in Fig. 4 is significantly stronger than the interference floor when both the DMI and IUI are cancelled. This shows that the IUI imposes a significant impact on target detection.

Figure 5 shows the processing results using the SSM shown in (12). It can be seen that the interference floor obtained by the SSM is larger than that by the BBB-MF.

In order to show the noise amplification effect of the SSM clearly, we redraw the processing results of beam 3 for the BBB-MF and SSM in Fig. 6. Figure 6a, b shows the range dimension projections of Fig. 3c and Fig. 5c. It can be clearly seen that the interference floor of the SSM is bigger than that of the BBB-MF. Moreover, it can be seen that, for the BBB-MF, target 3 is above the interference floor. However, target 3 is mixed within the interference floor for the SSM.

In the following, we examine the performance of the proposed BBB-MF in detection probability. We fix the simulation setups the same as above, except that we vary the SNR of target 1 from -50 to -10 dB. For each SNR, 100 Monte Carlo simulations are conducted and the detection probability of target 1 is evaluated. The constant false alarm rate (CFAR) method is used to perform target detection. The detection threshold is set to 12 dB. The number of guard cells at each side of the cell under test is set to 8, and that of the average cells is set to 16. The result is shown

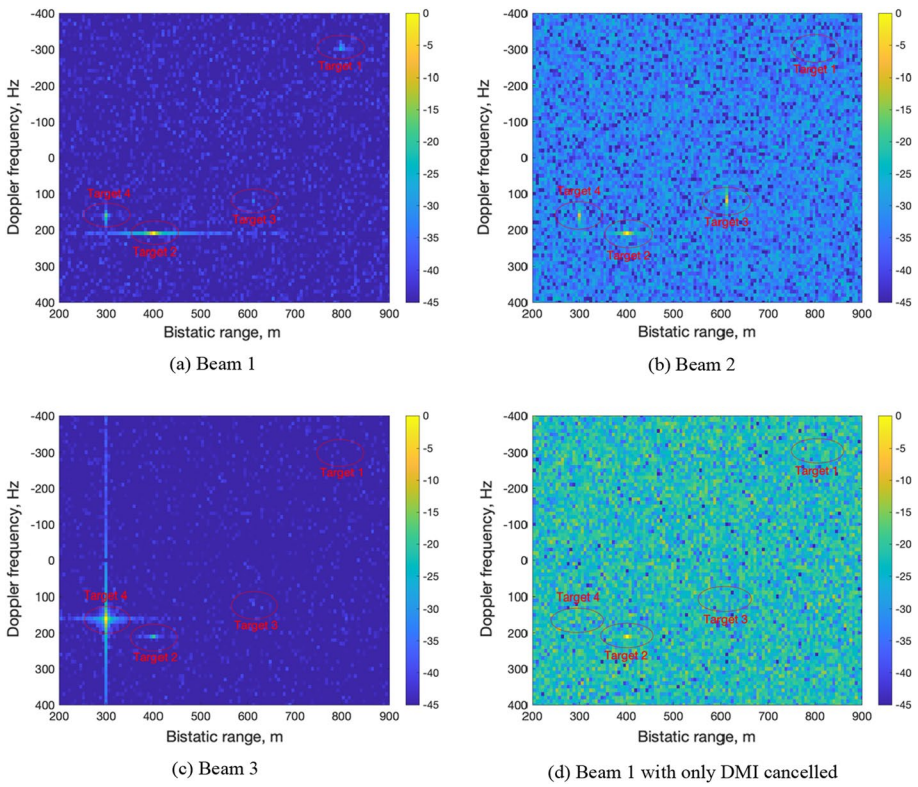

Fig. 5 Processing results by the SSM

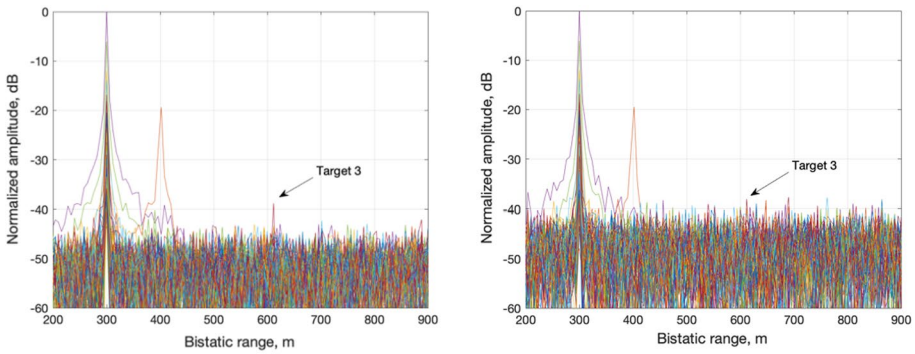

Fig. 6 Range dimension of the processing results by BBB-MF and SSM

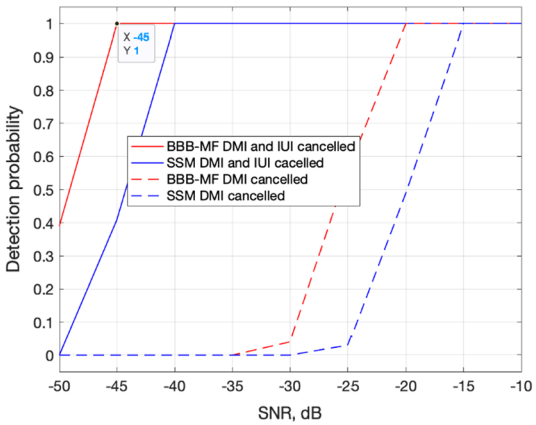

Fig. 7 Detection probability versus SNR

in Fig. 7. Figure 7 also shows the detection probability curve of the SSM, and the detection probability results of the BBB-MF and SSM with only the DMI cancelled. It is noted that the simulations here are performed by generating the channel estimate according to (8), the effectiveness of which has been verified by the simulations above. It is also noted that the SNRs in Fig. 7 are those before processing.

It can be seen from Fig. 7 that the BBB-MF has better detection performance than the SSM. Specifically, for the detection probability of above 0.8, the SSM with both DMI and IUI cancelled requires an SNR of above − 42 dB. However, the BBB-MF method with DMI and IUI cancelled only requires an SNR of above − 47 dB, which is 5 dB smaller than the SSM. A smaller SNR requirement means a larger detection range. It can also be seen that the IUI has a significant impact on the detection probability. For the detection probability of above 0.8, the BBB-MF with only DMI cancelled requires an SNR of above − 22 dB, and the SSM with only DMI cancelled requires an SNR of above − 17 dB, which are 25 dB bigger than the case where both the DMI and IUI are cancelled. Simulations demonstrate the superiority of the proposed methods.

5 Conclusion

In this paper, we discussed the passive radar sensing problem with the MU-MIMO-OFDM signal. We first developed the channel estimate model in the MU-MIMO-OFDM passive radar and then developed the BBB-MF for target sensing. The BBB-MF first uses the data symbols from the first beam to perform the matched filtering and then uses those from the second beam. This procedure repeats until the data symbols from the last beam are exploited. Performing the matched filtering beam by beam is similar to beam scanning in traditional radar. The proposed BBB-MF does not remove the data symbols from the channel estimate model but compensates the channel estimate model with the conjugate data symbols. Therefore, it has a smaller interference floor compared to the SSM and has good detection performance even for very small targets. We also discussed the DMI and IUI suppressing problem. Specifically, we analyzed the influence of IUI on target detection. It was shown that the IUI can degrade the target detection performance significantly. We proposed a joint DMI and IUI reduction method. The effectiveness of the proposed methods was verified through simulations.

Abbreviations

MU	Multi-users
MIMO-OFDM	Multiple-input multiple-output orthogonal frequency division multiplexing
5G	Fifth generation
BBB-MF	Beam-by-beam matched filter
BS	Base station
DMI	Direct and multipath interference
IUI	Inter-user interference
IoO	Illuminator of opportunity
FM	Frequency modulation
DAB	Digital audio broadcasting
DVB	Digital video broadcasting
GSM	Global system for mobile communications
WLAN	Wireless local area network
LTE	Long-term evolution
SINR	Signal-to-interference plus noise ratio
FFT	Fast Fourier transform
LMMSE	Linear minimum mean square error
SSM	Signal stripping method
SNR	Signal-to-noise ratio
GoB	Grid of beam
QPSK	Quadrature phase shift keying
64-QAM	64-Quadrature amplitude modulation
256-QAM	256-Quadrature amplitude modulation

Acknowledgements
The authors would like to thank the committee of the National Natural Science Foundation of China (NSFC).

Author contributions
XL, BL, and WF contributed to conceptualization, writing—review and editing, and validation; XL contributed to methodology, software, writing—original draft preparation, project administration, and funding acquisition; All authors have read and agreed to the published version of the manuscript.

Funding
This research is funded by the National Natural Science Foundation of China (NSFC), Grant No. 62101501.

Availability of data and materials
Not applicable.

Declarations

Ethics approval and consent to participate
Not applicable.

Consent for publication
Not applicable.

Competing interests
The authors declare that they have no competing interests.

Received: 26 May 2022 Accepted: 14 November 2022
Published online: 26 November 2022

References

1. H.D. Griffiths, C.J. Baker, Passive coherent location radar systems. Part 1: Performance prediction. IEE Proc. Radar Sonar Navig. **152**(3), 153–159 (2005)
2. Y. Zhu et al., Decomposed POMDP optimization-based sensor management for multi-target tracking in passive multi-sensor systems. IEEE Sens. J. **22**(4), 3565–3578 (2022)
3. Y. Junkun et al., Radar sensor network resource allocation for fused target tracking: a brief review. Inf. Fusion **86**(87), 104–115 (2022)
4. P.E. Howland, D. Maksimiuk, G. Reitsma, FM radio based bistatic radar. IEE Proc. Radar Sonar Navig. **152**(3), 107–115 (2005)
5. F. Colone, C. Bongioanni, P. Lombardo, Multifrequency integration in FM radio-based passive bistatic radar. Part I: Target detection. IEEE Aerosp. Electron. Syst. Mag. **28**(4), 28–39 (2013)
6. D.W. O'Hagan, C.J. Baker, Passive bistatic radar (PBR) using FM radio illuminators of opportunity. in *2008 new trends for environmental monitoring using passive systems*. (IEEE, 2008).
7. P.F. Howland, Target tracking using television-based bistatic radar. IEE Proc. Radar Sonar Navig. **146**(3), 166–174 (1999)
8. A. Zaimbashi, Target detection in analog terrestrial TV-based passive radar sensor: joint delay-Doppler estimation. IEEE Sens. J. **17**(17), 5569–5580 (2017)
9. J.E. Palmer et al., DVB-T passive radar signal processing. IEEE Trans. Signal Process. **61**(8), 2116–2126 (2012)
10. S. Choi et al., Approaches to Cartesian data association passive radar tracking in a DAB/DVB network. IEEE Trans. Aerosp. Electron. Syst. **50**(1), 649–663 (2014)
11. T. Shan et al., Efficient architecture and hardware implementation of coherent integration processor for digital video broadcast-based passive bistatic radar. IET Radar Sonar Navig. **10**, 97–106 (2016)
12. D.K.P. Tan et al., Passive radar using global system for mobile communication signal: theory, implementation and measurements. IEE Proc. Radar Sonar Navig. **152**(3), 116–123 (2005)
13. P. Krysik et al., Velocity measurement and traffic monitoring using a GSM passive radar demonstrator. IEEE Aerosp. Electron. Syst. Mag. **27**(10), 43–51 (2012)
14. D. Pastina et al., Passive radar imaging of ship targets with GNSS signals of opportunity. IEEE Trans. Geosci. Remote Sens. **59**(3), 2627–26424 (2020)
15. S.A. Kaiser, A.J. Christianson, R.M. Narayanan, Multistatic Doppler estimation using global positioning system passive coherent location. IEEE Trans. Aerosp. Electron. Syst. **55**(6), 2978–2991 (2019)
16. Z. Li et al., BeiDou-based passive multistatic radar maritime moving target detection technique via space-time hybrid integration processing. IEEE Trans. Geosci. Remote Sens. **60**, 1–13 (2022)
17. X. Lyu et al., Ambiguity function of Inmarsat BGAN signal for radar application. Electron. Lett. **52**(18), 1557–1559 (2016)
18. X. Lyu et al., Ambiguity function of Iridium signal for radar application. Electron. Lett. **521**(9), 1631–1633 (2016)
19. F. Colone et al., WiFi-based passive bistatic radar: Data processing schemes and experimental results. IEEE Trans. Aerosp. Electron. Syst. **48**(2), 1061–1079 (2012)
20. F. Colone et al., WiFi-based passive ISAR for high-resolution cross-range profiling of moving targets. IEEE Trans. Geosci. Remote Sens. **52**(6), 3486–3501 (2013)
21. D. Pastina et al., Parasitic exploitation of Wi-Fi signals for indoor radar surveillance. IEEE Trans. Veh. Technol. **64**(4), 1401–1415 (2015)
22. W. Li et al., Passive WiFi radar for human sensing using a stand-alone access point. IEEE Trans. Geosci. Remote Sens. **59**(3), 1986–1998 (2020)
23. H. Sun, L.G. Chia, S.G. Razul, Through-wall human sensing with WiFi passive radar. IEEE Trans. Aerosp. Electron. Syst. **57**(4), 2135–2148 (2021)
24. A.A. Salah et al., Experimental study of LTE signals as illuminators of opportunity for passive bistatic radar applications. Electron. Lett. **50**(7), 545–547 (2014)
25. A. Evers, and J.A. Jackson, Analysis of an LTE waveform for radar applications. in *2014 IEEE Radar Conference*. (IEEE, 2014)
26. C. Klöck, V. Winkler, M. Edrich, LTE-signal processing for passive radar air traffic surveillance. in *2017 18th international radar symposium (IRS)*. (IEEE, 2017)
27. P. Lingadevaru et al., Analysis of 5G new radio waveform as an illuminator of opportunity for passive bistatic radar. in *2021 national conference on communications (NCC)*. (IEEE, 2021)
28. P. Samczyński et al., 5G Network-Based Passive Radar." IEEE Transactions on Geoscience and Remote Sensing 60 (2022).
29. A. Xiaofeng et al., Passive detection experiment of UAV based on 5G new radio signal. in *2021 photonics & electromagnetics research symposium (PIERS)*. (IEEE, 2021)
30. E. Dahlman, S. Parkvall, J. Skold, *5G NR: the next generation wireless access technology*. (Academic press, UK)
31. A. Zaidi et al. *5G physical layer principles, models and technology components*. (Academic press, UK)
32. M.E. Davis, *Advances in bistatic radar*. vol. 2. (SciTech Publishing, 2007)
33. M. Malanowski, *Signal processing for passive bistatic radar*. (Artech House, 2019)

34. C.R. Berger et al., Signal processing for passive radar using OFDM waveforms. IEEE J. Select. Top. Signal Process. **4**(1), 226–238 (2010)
35. G. Chabriel, J. Barrère, Adaptive target detection techniques for OFDM-based passive radar exploiting spatial diversity. IEEE Trans. Signal Process. **65**(22), 5873–5884 (2017)
36. Y. Liu et al., Evaluation of clutter suppression in CP-OFDM-based passive radar. IEEE Sens. J. **19**(14), 5572–5586 (2019)
37. G. Barb, M. Otesteanu. Digital GoB-based Beamforming for 5G communication systems. in *2020 international symposium on antennas and propagation (ISAP)*. (IEEE, 2021)
38. L.M. Hoang et al., Suppression of multiple spatially jammers. IEEE Trans. Veh. Technol. **70**, 10489–10500 (2021)
39. M.L. Rahman et al., Framework for a perceptive mobile network using joint communication and radar sensing. IEEE Trans. Aerosp. Electron. Syst. **56**(3), 1926–1941 (2019)
40. J.A. Zhang et al., Signal stripping based sensing parameter estimation in perceptive mobile networks. in *2017 IEEE-APS topical conference on antennas and propagation in wireless communications (APWC)*. (IEEE, 2017)
41. R.S. Thoma et al., Cooperative passive coherent location: a promising 5G service to support road safety. IEEE Commun. Mag. **57**(9), 86–92 (2019)
42. F. Colone et al., A multistage processing algorithm for disturbance removal and target detection in passive bistatic radar. IEEE Trans. Aerosp. Electr. Syst. **45**(2), 698–722 (2009)

Publisher's Note